AD-A271 696

'ATION PAGE

Form Approved
OMB No. 0704-0188

1. AGENCY USE ONLY (Leave blank)	2. REPORT DATE	3. REPORT TYPE AND DATES COVERED

4. TITLE AND SUBTITLE

State-selected Chemical Reaction Dynamics at the S Matrix Level: Final -state Specificities of Near-Threshold Processes at Low and High Energies

5. FUNDING NUMBERS

DAAL03-89-C-0038

(2)

6. AUTHOR(S)

David C. Chatfield, Donald G. Truhlar, and David W. Schwenke

7. PERFORMING ORGANIZATION NAME(S) AND ADDRESS(ES)

University of Minnesota - School of Mathematics
127 Vincent Hall
Minneapolis, MN 55455

8. PERFORMING ORGANIZATION REPORT NUMBER

9. SPONSORING/MONITORING AGENCY NAME(S) AND ADDRESS(ES)

U. S. Army Research Office
P. O. Box 12211
Research Triangle Park, NC 27709-2211

10. SPONSORING/MONITORING AGENCY REPORT NUMBER

ARO 27747.16-MA-COE

11. SUPPLEMENTARY NOTES

The view, opinions and/or findings contained in this report are those of the author(s) and should not be construed as an official Department of the Army position, policy, or decision, unless so designated by other documentation.

12a. DISTRIBUTION/AVAILABILITY STATEMENT

Approved for public release; distribution unlimited.

12b. DISTRIBUTION CODE

13. ABSTRACT *(Maximum 200 words)*

State-to-state reaction probabilities are found to be highly final-state specific at state-selected threshold energies for the reactions $O + H_2 \rightarrow OH + H$ and $H + H_2 \rightarrow H_2 + H$. The study includes initial rotational states with quantum numbers 0–15, and the specificity is especially dramatic for the more highly rotationally excited reactants. The analysis is based on accurate quantum mechanical reactive scattering calculations. Final-state specificity is shown in general to increase with the rotational quantum number of the reactant diatom, and the trends are confirmed for both zero and nonzero values of the total angular momentum.

14. SUBJECT TERMS			15. NUMBER OF PAGES
			16. PRICE CODE
17. SECURITY CLASSIFICATION OF REPORT	18. SECURITY CLASSIFICATION OF THIS PAGE	19. SECURITY CLASSIFICATION OF ABSTRACT	20. LIMITATION OF ABSTRACT
UNCLASSIFIED	UNCLASSIFIED	UNCLASSIFIED	UL

State-selected chemical reaction dynamics at the *S* matrix level: Final-state specificities of near-threshold processes at low and high energies

David C. Chatfield and Donald G. Truhlar
Department of Chemistry, Supercomputer Institute, and Army High-Performance Computing Research Center, University of Minnesota, Minneapolis, Minnesota 55455-0431

David W. Schwenke
NASA Ames Research Center, Moffet Field, California 94035

(Received 8 October 1991; accepted 2 December 1991)

State-to-state reaction probabilities are found to be highly final-state specific at state-selected threshold energies for the reactions $O + H_2 \rightarrow OH + H$ and $H + H_2 \rightarrow H_2 + H$. The study includes initial rotational states with quantum numbers 0–15, and the specificity is especially dramatic for the more highly rotationally excited reactants. The analysis is based on accurate quantum mechanical reactive scattering calculations. Final-state specificity is shown in general to increase with the rotational quantum number of the reactant diatom, and the trends are confirmed for both zero and nonzero values of the total angular momentum.

I. INTRODUCTION

Quantum mechanical scattering theory allows us to study many characteristics of state-to-state dynamical processes more systematically and at a greater level of detail than is currently feasible by experiment. A classic example is the detailed analysis of statistical vs state-specific behavior in individual elements of the scattering matrix (*S* matrix) for inelastic scattering by Lester and Bernstein.[1] At the level of the *S* matrix, we can observe transition probabilities between individual channels specified completely by their full sets of quantum numbers—the ultimate level of resolution allowed by quantum mechanics. The study of transition probabilities at this most detailed level is the eventual limit of any increasingly exact dynamical theory of chemical processes and—in addition—it is sometimes directly relevant to certain modern experiments involving laser-prepared initial states and state-specific product detection. In the present paper, we report an interesting and qualitatively unexpected behavior observed at the *S* matrix level for reactive scattering involving reactants with varying levels of internal excitation, including highly rotationally excited states whose reactions are hard to study experimentally.

We have found that state-selected reactivity is characterized by a surprisingly high degree of final-state specificity at energies near state-selected reaction thresholds for the reactions $O + H_2 \rightarrow OH + H$ and $H + H_2 \rightarrow H_2 + H$. In many cases, we find that 50% or more of the state-selected reactive flux is into three or fewer final states and 75% or more is into six or fewer final states, even when up to 78 final states are open. The trends have been confirmed for both zero and nonzero values of the total angular momentum. This is an exciting result because such a high degree of final-state specificity is unexpected, particularly at high energy.

II. CALCULATIONS

The reactive scattering calculations for $O + H_2$ were carried out with the realistic Johnson–Winter–Schatz (JWS) potential energy surface,[2] and the calculations for $H + H_2$ used the highly accurate double many-body expansion (DMBE) surface.[3] The calculations were performed using a linear algebraic variational basis-set method based on the generalized Newton variational principle for the amplitude density.[4] For both reactions, convergence of the state-to-state reaction probabilities was estimated by comparing the production runs to convergence checks in which a sufficient subset of basis set and numerical parameters was varied to check *all* sources of possible error in the solution of the Schrödinger equation. The average deviation of state-to-state reaction probabilities greater than 10^{-4} between these two runs was 0.1%–3%, depending on the system, energy, and angular momentum for the results discussed in this paper. Detailed presentations of basis sets and numerical parameters for these systems have been[5,6] and will be[7] presented elsewhere. We simply mention that the number of coupled channels (after taking advantage of total angular momentum J, parity P, and arrangement symmetry to form linear-combination basis functions that are maximally decoupled[4]) for the calculations in this paper ranges from 132 (at low energies) to 196 (at high energies) for $O + H_2$ and from 162 (for $J = 0$) to 260 (for $J = 4$ and $P = +1$) for $H + H_2$ at all energies.

A state-selected reaction probability $P^R_\gamma(E,J)$ for initial state γ, total energy E, and total angular momentum J is defined as the sum of state-to-state reaction probabilities $P^R_{\gamma\gamma'}(E,J)$ over all final states, where $\gamma(\gamma')$ is a set of diatom quantum numbers for reactants (products)

$$P^R_\gamma = \sum_{\gamma'} P^R_{\gamma\gamma'}(E,J). \tag{1}$$

The set γ consists of quantum numbers for arrangement (α), vibration (v), and rotational angular momentum (j), and the superscript R denotes that the final arrangement $\alpha_{\gamma'}$ is different from the initial arrangement α_γ. In both cases studied here, there are two identical final reactive arrangements ($\alpha = 2$ and 3) since H_2 is homonuclear and $P^R_{\gamma\gamma'}$ denotes the

 0021-9606/92/064313-11$06.00

reaction probability for either product arrangement, say $\alpha = 2$. (None of our conclusions would be changed if we summed over $\alpha = 2$ and 3, but it is necessary to make a consistent choice for tabulation and discussion purposes, and we chose to deal with the individual $\alpha = 1 \rightarrow \alpha' = 2$ probabilities.) Thus, if $S^{JP}_{\gamma' l' \gamma l}(E)$ denotes an S matrix element for total energy E, total angular momentum J, parity P, and initial and final orbital angular momentum of relative translation l and l', then

$$P^R_{\gamma\gamma'} = \frac{1}{2\min(J,j)+1} \sum_{n \in \mathcal{S}(\gamma)} \sum_{n' \in \mathcal{S}(\gamma')} P^R_{nn'}(E,J), \quad (2)$$

where n denotes a channel, i.e., a combination of values γ_n and l_n of γ and l, $\mathcal{S}(\gamma)$ denotes the set of all channels which correspond to state γ, and $P^R_{nn'}$ is a channel-to-channel reaction probability defined by

$$P^R_{nn'} = |S^{JP}_{\gamma_{n'} l_{n'} \gamma_n l_n}(E)|^2. \quad (3)$$

Note that a particular combination of γ_n and l_n uniquely specifies the parity P, so it is not necessary to include a summation over the parity P on the right-hand side of Eq. (3). The sum over n in Eq. (2) automatically picks up contributions from both parities.

For total angular momentum J equal to zero, $P^R_{nn'}$ is the same as $P^R_{\gamma\gamma'}$ since there is only one allowed value of l for each γ and one allowed value of l' for each γ'; thus we can use either the state-selected or the channel-selected language for $J = 0$. In the case of $J \neq 0$, state-selected and channel-selected results differ and we will consider both; the state-selected results are more closely related to observables when scattering angles are not detected, and the channel-selected results are of special interest because (as stated in the Introduction) they provide the ultimate level of detail about reaction dynamics that is allowed by quantum mechanics.

For the purposes of this article, we define a state-selected reaction threshold $E_{\rm thr}$ as the first maximum in the density of state-selected density reaction probability $\rho_\gamma(E,J)$, which is defined as the energy derivative of $P^R_\gamma(E,J)$,[8]

$$\rho_\gamma = \frac{d}{dE} P^R_\gamma(E,J), \quad (4)$$

and similarly a channel-selected reaction threshold is the first maximum of

$$\rho_n = \frac{d}{dE} P^R_n(E,J), \quad (5)$$

where $P^R_n(E,J)$, in analogy to $P^R_\gamma(E,J)$, is a channel-selected reaction probability given by

$$P^R_n = \sum_{n'} P^R_{nn'}(E,J). \quad (6)$$

We will also discuss analogous quantities for final states. We define a final-state-selected reaction probability $P^R_{\gamma'}$ as

$$P^R_{\gamma'} = \sum_{\gamma} P^R_{\gamma\gamma'}(E,J) \quad (7)$$

and a density of final-state-selected reaction probability $\rho_{\gamma'}(E,J)$ as

$$\rho_{\gamma'} = \frac{d}{dE} P^R_{\gamma'}(E,J), \quad (8)$$

For final states, $E_{\rm thr}$ is defined as the energy of the first maximum in $\rho_{\gamma'}(E,J)$.

The present paper is based on calculations for $O + H_2$ with $J = 0$ and $H + H_2$ with $J = 0$ and $J = 4$ over a wide range of energies ($E = 0.60$–1.90 eV for $O + H_2$ and 0.80–1.60 eV for $H + H_2$). We examined several initial states and channels for each reaction and found the thresholds as just defined for the $J = 0$ calculations. We determined the threshold energies for $H + H_2$ with $J = 4$ by adding an energy for rotation $BJ(J+1) = 0.026$ eV to the $J = 0$ energies, using a value of $10.6\ {\rm cm}^{-1} = 0.001\ 31$ eV for B determined from a previous analysis of quantized transition state energies.[8] The $J = 4$ analysis presented here was carried out for the energies nearest these threshold energies on a preselected grid of energies that span the region of interest. The energy used was within 0.016 eV of the threshold energy calculated using B in all cases. We then examined the distributions of final states or channels in each of the $J = 0$ or 4 threshold calculations in order to examine the final-state specificities that form the title subject of this article.

The central quantities under study here are product distribution specificities for various initial states or channels at their reaction thresholds. Thus we define normalized product distributions as

$$D(v',j'|v,j) = \frac{P^R_{\gamma\gamma'}}{P^R_\gamma} \quad (9)$$

and

$$D(v',j',l'|v,j,l) = \frac{P^R_{nn'}}{P^R_n}. \quad (10)$$

(Since $P^R_{\gamma\gamma'}$ and $P^R_{nn'}$ include only a particular $\alpha \rightarrow \alpha'$ pair, namely $1 \rightarrow 2$, the denominators are not unity.) We also define a partially summed distribution

$$D(v'|v,j) = \sum_{j'} D(v',j'|v,j) \quad (11)$$

in order to study the specificity of reaction into each final vibrational level.

III. RESULTS AND DISCUSSION

III. A. State-selected specificities for $O + H_2$

Table I summarizes the specificity of reaction ($\alpha = 1 \rightarrow \alpha' = 2$) out of initial states in the ground vibrational manifold for the $O + H_2$ reaction with total angular momentum equal to zero. The first four columns give the value of the initial rotational quantum number j, the energy $E_{\rm thr}$ of the state-selected threshold (relative to the potential energy of infinitely separated reactants at classical equilibrium), the relative translational energy $E_{\rm rel,thr}$, and the number of open final states $N_{\rm open}(E)$ with $\alpha' = 2$. More precisely, we define the state-selected threshold energy $E_{\rm thr}$ as the first maximum of $\rho_n(E,J)$, and the energy $E_{\rm rel,thr}$ is the relative translational energy for the given initial state and total energy $E_{\rm thr}$. To create the table, the final states with $\alpha' = 2$ were ordered by decreasing magnitude of the normalized state-to-state product conditional probabilities $D(v',j'|v,j)$. These conditional probabilities were then summed, beginning with

TABLE I. Final-state specificity of reaction out of initial states in the $v = 0$ manifold for the $O + H_2$ reaction with $J = 0$.

j	E_{thr} (eV)	$E_{rel,thr}$ (eV)	N_{open}	25% N	25% F	50% N	50% F	75% N	75% F	Dominant (v',j'), $D(v',j'\|0,j)$[a]			
0	0.69	0.42	12	2	0.17	3	0.25	5	0.42	(0,4) 18	(0,3) 17	(0,5) 17	(0,2) 14
1	0.69	0.41	12	2	0.17	3	0.25	5	0.42	(0,4) 18	(0,5) 17	(0,3) 17	(0,2) 13
2	0.69	0.38	12	2	0.17	3	0.25	5	0.42	(0,5) 18	(0,4) 17	(0,6) 16	(0,3) 14
3	0.70	0.34	12	2	0.17	4	0.33	6	0.50	(0,5) 17	(0,4) 17	(0,6) 15	(0,3) 14
4	0.71	0.30	13	2	0.15	4	0.31	6	0.46	(0,5) 17	(0,6) 16	(0,4) 15	(0,7) 13
5	0.89	0.41	23	2	0.09	3	0.13	4	0.17	(0,9) 23	(0,10) 23	(0,8) 16	(0,11) 15
6	0.95	0.38	25	2	0.08	3	0.12	6	0.24	(0,11) 22	(0,10) 19	(0,12) 16	(0,9) 10
7	0.96	0.29	26	2	0.09	3	0.12	7	0.27	(0,12) 21	(0,11) 19	(0,13) 12	(0,10) 9
8	1.10	0.33	30	2	0.07	4	0.13	7	0.23	(0,14) 21	(0,13) 18	(1,8) 11	(0,15) 9
9	1.23	0.34	37	2	0.05	3	0.08	6	0.16	(0,15) 21	(0,16) 19	(1,11) 16	(1,10) 12
10	1.38	0.36	48	2	0.04	3	0.06	6	0.13	(0,17) 23	(1,13) 19	(0,18) 13	(0,16) 10
11	1.48	0.32	52	2	0.04	3	0.06	6	0.12	(1,14) 21	(0,18) 17	(1,15) 16	(0,19) 14
12	1.60	0.30	58	1	0.02	3	0.05	7	0.12	(1,16) 29	(0,20) 16	(0,19) 11	(1,15) 6
13	1.72	0.27	70	2	0.03	3	0.04	8	0.11	(1,17) 20	(1,18) 19	(0,21) 15	(1,15) 7
14	1.86	0.25	78	1	0.01	4	0.05	10	0.13	(1,19) 31	(0,22) 10	(1,17) 6	(0,23) 6

[a]The four final states which contribute most to P_γ^R and their normalized conditional probabilities expressed as percentages, $D(v',j'|0,j) \times 100\%$, listed in order of the size of $D(v',j'|0,j)$, beginning with the greatest contributor.

the largest, until the sum was 0.25 or greater. The number of contributors required to reach this value of the sum is listed in the column labeled $N(25\%)$. Similarly, the number of states contributing when the sum reached 0.50 and 0.75 are shown in the columns labeled $N(50\%)$ and $N(75\%)$. Also shown are columns headed $F(25\%)$, $F(50\%)$, and $F(75\%)$, which denote what fraction of the N_{open} energetically accessible states contribute these percentages of the normalized distribution, i.e.,

$$F(x\%) = \frac{N(x\%)}{N_{open}}. \tag{12}$$

Finally, the four final states which contribute most to the state-selected reaction probability are listed at the right, together with their normalized conditional probabilities expressed as percentages.

It is seen in Table I that as j is varied from 0 to 14, the state-selected threshold energy increases from 0.69 to 1.86 eV and the number of final OH states open at threshold increases from 12 to 78. Nevertheless, for all j, at most two final states are required to account for 25% of the state-selected reactive flux, and for $j = 12$ and 14, a single final state accounts for over 25% of the flux. Thus much of the state-selected reactivity is very final-state specific, particularly at high j. Perhaps even more dramatic is that in most cases, three final states account for more than half of the flux, and about six states account for 75% of the flux. The amount of flux into the single one or two greatest-contributing final states becomes larger for high-energy (i.e., high-j) thresholds, while the remaining flux tends to be spread among more final states for these thresholds, as evidenced by the larger values (7, 8, and 10) of $N(75\%)$ for the three states with highest j. The fractions $F(x\%)$ for all three values of x show that the reactive flux becomes focused into a *smaller* fraction of the open final states as j is *increased*.

These trends are demonstrated in Figs. 1(a)–1(c), in which the value of $P_{\gamma\gamma'}^R$ at the state-selected threshold energy is plotted vs j' for initial states (0,0), (0,8), and (0,14), where the first number in parentheses denotes v and the second denotes j. It is seen that as initial j is increased within the ground vibrational manifold, the distribution $D(v',j'|0,j)$ becomes peaked about a narrower range of j' values, and vibrationally nonadiabatic transitions become more important.

Threshold reactivity for the $v = 1$ manifold is summarized in Table II. The vibrationally excited states are even more final-state specific than the ground vibrational states. For four of the 12 initial states listed in Table II, a single final state accounts for over 25% of the reactive flux. The three highest-j states are among these four, which confirms the remarkable degree of final-state specificity at high j noted above. This phenomenon is demonstrated for the initial state (1,10) in Fig. 2, in which $P_{\gamma\gamma'}^R$ is plotted vs j'. As for initial state (0,14) [Fig. 1(c)], $D(v',j'|1,10)$ is peaked about a narrow range of j' values for the dominant v', and nonadiabatic transitions dominate the state-selected reactivity.

The larger values of the product distribution specificities $D(v',j'|v,j)$ tend to be very simple functions of j', for a given v', with a single maximum. One might ask whether this is a consequence of a simple dependence on final internal energy. For example, consider the four most important final states in Table I for $j = 11$, 12, and 13. If the most important $(v' = 0, j')$ state were always the one intermediate in energy between the two most important $(v' = 1, j')$ states, then we would predict the j' values of 20, 21, and 22 to be the most important ones in the $v' = 0$ manifold for $j = 11$, 12, and 13, respectively, but instead the table shows that the dominant $(v' = 0, j')$ state is $j' = 18$, 20, and 21 in these three cases. In addition, some states with very similar internal energies to the dominant (v', j') state have very small probabilities. For example, consider the $j = 13$ case of Table I again. In this case, the four final states with the largest values of

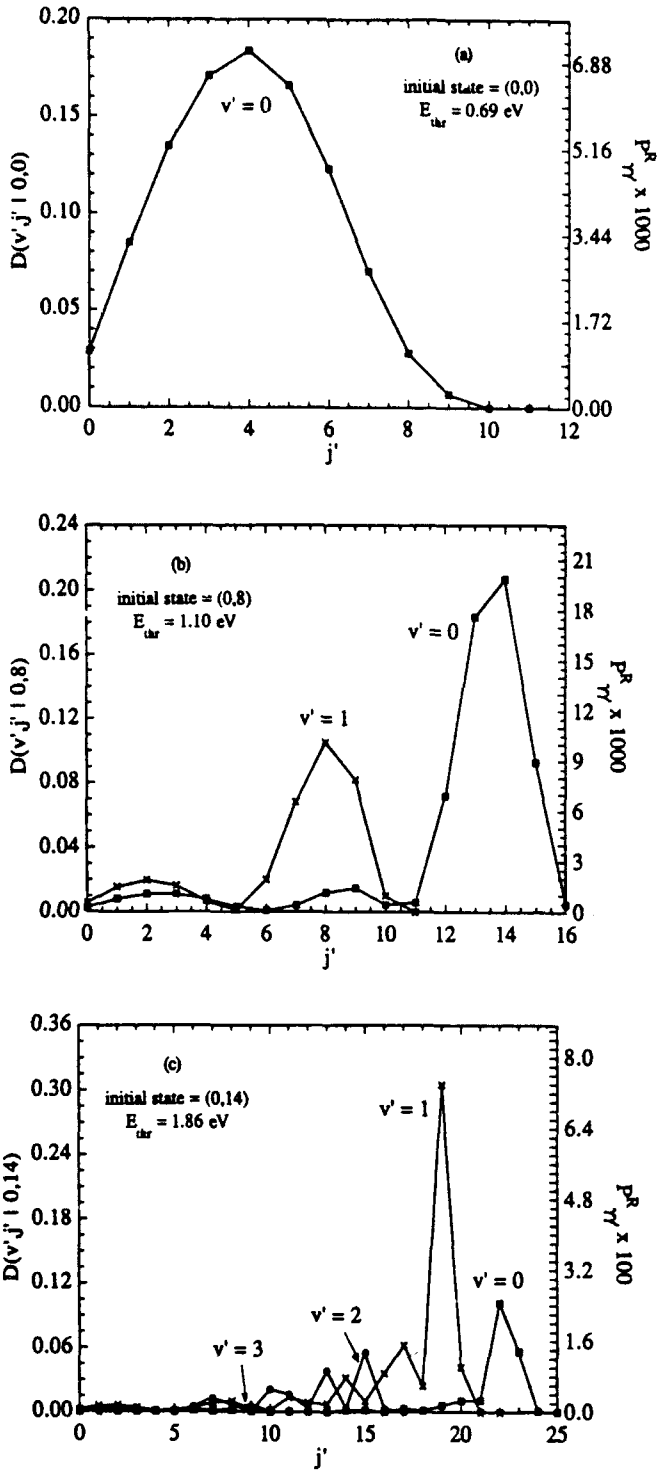

FIG. 1. Normalized product distribution $D(v',j'|v,j)$ and state-to-state reaction probabilities $P^R_{v'}$ vs final rotational quantum number j' for the $O + H_2$ reaction with $J = 0$ for (a) initial state (0,0) at energy $E_{thr} = 0.69$ eV; (b) initial state (0,8) at 1.10 eV; and (c) initial state (0,14) at 1.86 eV.

$D(v',j'|0,13)$, listed in Table I, have internal energies varying between 1.31 and 1.52 eV. There are seven other final states with internal energies in this range but the average value of $D(v',j'|0,13)$ for these seven states is only 2, as compared to 15 for the four most important states.

Thus the reactive flux is not simply concentrated into those product states whose internal energies are closest to the internal energy of the reactant state. In Table III, the internal energy and the state-selected threshold energy are tabulated for initial states (0,11), (0,12), and (0,13) and, for comparison, for selected final states having large conditional probabilities for reaction out of these three initial states. (The four largest conditional probabilities for each initial state are listed in Table I.) For those final states corresponding to the largest conditional probabilities, there is a better correlation between the state-selected thresholds, defined as explained above in terms of Eqs. (4) and (8), for the initial and final states than between the internal energies of the initial and final states. Note, for instance, that for initial state (0,11), the largest conditional probabilities corresponding to final states in the $v' = 1$ manifold are for final states (1,14) and (1,15) (21% and 16%, respectively). These are the two final states whose state-selected thresholds (1.410 and 1.484 eV), are closest to the state-selected threshold for initial state (0,11) (1.484 eV). The internal energies of final states (1,14) and (1,15) though, 1.293 and 1.306 eV, are considerably higher than the internal energy of initial state (0,11) (1.157 eV). The two final states in the $v' = 1$ vibrational manifold whose internal energies are closest to the internal energy of initial state (0,11) are final states (1,12) and (1,13). However, their thresholds are much lower in energy than the threshold for initial state (0,11) and the conditional probabilities $D(1,12|0,11)$ and $D(1,13|0,11)$ are quite small, 1% and 3%.

A particularly striking example of this trend is seen for initial state (0,13). The largest conditional probability corresponding to a final state in the $v' = 0$ vibrational manifold is 15%, for final state (0,21). Initial state (0,13) and final state (0,21) have nearly identical state-selected thresholds (1.718 and 1.716 eV). The conditional probability corresponding to final state (0,22), on the other hand, is only 4%, even though initial state (0,13) and final state (0,22) have nearly the same internal energies (1.454 and 1.453 eV). The threshold for final state (0,22) is 1.848 eV, much higher than that for initial state (0,13).

The fact that the threshold energies for initial and final states with large conditional probabilities are in better agreement than the internal energies of the states suggests that the thresholds are correlated with transition states through which the reactive flux is channeled. This view is in agreement with the work in Refs. 5 and 8, where it is shown that quantized transition states control the chemical reactivity for the reaction $H + H_2 \rightarrow H_2 + H$.

Tables I and II demonstrate that for both the $v = 0$ and 1 vibrational manifolds, the state-selected threshold reactivity is primarily vibrationally adiabatic at low to moderate j (which also corresponds to low to moderate energy); i.e., the important final states tend to have the same vibrational quantum number as the initial state. As noted above for selected initial states, vibrational nonadiabaticity becomes more important at higher j levels. For initial states with $v = 0$ and $j = 11$–14, the single most important final state has $v' = 1$; for initial states with $v = 1$ and $j = 9$–11, the single most important final state has $v' = 2$.

TABLE II. Final-state specificity of reaction out of initial states in the $v = 1$ manifold for the $O + H_2$ reaction with $J = 0$.

j	E_{thr} (eV)	$E_{rel,thr}$ (eV)	N_{open}	25% N	25% F	50% N	50% F	75% N	75% F	Dominant (v',j'), $D(v',j'\|1,j)$[a]
0	0.97	0.17	26	2	0.08	3	0.12	5	0.19	(1,3) 19 (1,4) 19 (1,2) 16 (1,5) 13
1	0.97	0.17	26	2	0.08	3	0.12	5	0.19	(1,3) 19 (1,4) 19 (1,2) 16 (1,5) 14
2	0.97	0.15	26	2	0.08	3	0.12	5	0.19	(1,3) 19 (1,4) 19 (1,2) 16 (1,1) 14
3	0.98	0.11	26	2	0.08	3	0.12	5	0.19	(1,4) 19 (1,3) 19 (1,2) 15 (1,5) 14
4	1.14	0.12	32	2	0.06	3	0.09	6	0.19	(1,8) 24 (1,9) 19 (1,7) 17 (1,10) 7
5	1.22	0.23	37	2	0.05	3	0.08	7	0.19	(1,10) 24 (1,11) 17 (1,9) 17 (1,8) 7
6	1.29	0.22	42	2	0.05	3	0.07	7	0.17	(1,12) 25 (1,11) 22 (1,7) 9 (1,6) 6
7	1.38	0.22	48	1	0.02	3	0.06	7	0.15	(1,13) 32 (1,12) 13 (1,14) 12 (2,5) 7
8	1.47	0.21	52	2	0.04	3	0.06	8	0.15	(1,14) 20 (1,15) 15 (2,8) 15 (2,9) 11
9	1.56	0.18	56	1	0.02	3	0.05	7	0.13	(2,10) 28 (1,16) 17 (1,15) 10 (2,11) 9
10	1.66	0.16	65	1	0.02	3	0.05	7	0.11	(2,12) 37 (1,17) 12 (2,11) 9 (2,9) 8
11	1.83	0.21	76	1	0.01	3	0.04	9	0.12	(2,14) 26 (2,15) 16 (1,19) 13 (0,21) 5

[a] The four final states which contribute most to $P^R_{v'}$ and their normalized conditional probabilities expressed as percentages, $D(v',j'|1,j) \times 100\%$, listed in order of the size of $D(v',j'|1,j)$, beginning with the greatest contributor.

Trends in vibrational level specificity for initial states in the $v = 0$ and 1 vibrational manifolds are displayed in Figs. 3 and 4. For initial states in the ground vibrational manifold, threshold reactivity is vibrationally adiabatic up to $j = 5$ ($E_{thr} = 0.89$ eV) since the threshold for reaction into $v = 1$ is 0.97 eV. Above $j = 5$, the fraction of reactivity that accesses final $v' = 1$ states increases regularly, until by $j = 11$, a greater fraction of the flux goes into final $v' = 1$ states than final $v' = 0$ states. Reaction into $v' = 2$ and 3 final states remains small even at energies considerably above the thresholds for reaction into these vibrational levels.

A similar trend is seen for initial states in the $v = 1$ vibrational manifold. Threshold reactivity into $v' = 0$ final states remains relatively constant over the entire range of j values, varying between 8% and 15% of the reactive flux. Beginning with $j = 6$(1.29 eV), reaction into final $v' = 2$ states increases regularly until $j = 10$ and then drops off as reaction begins to occur into $v' = 3$ states. By $j = 9$, a greater fraction of the flux out of initial $v = 1$ states goes into final $v' = 2$ states than into $v' = 1$ states.

It is seen in Tables I and II that initial states within a given vibrational manifold whose thresholds occur at nearly the same energy [(0,0), (0,1), (0,2), (0,3), and (0,4); (0,5), (0,6), and (0,7); or (1,0), (1,1), (1,2), and (1,3)] send flux to the same or nearly the same set of final states. This phenomenon may be due to the dominance of the individual threshold reactivities of a set of initial states by the same energy level of the transition state.[8] Like other resonances, quantized transition state thresholds are intermediates, and so the threshold flux through a quantized transition state tends to lose memory of its particular state of origin.

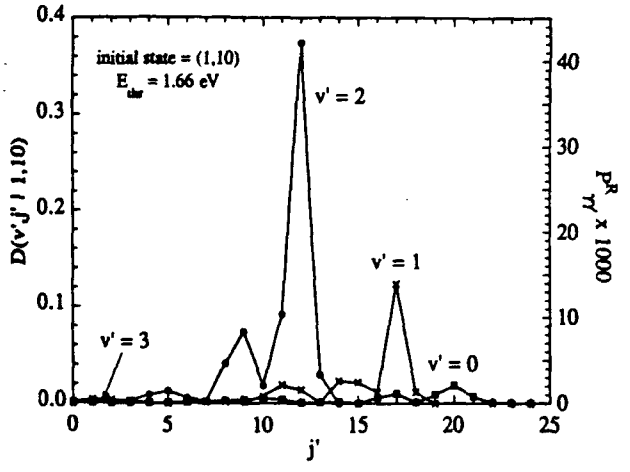

FIG. 2. Normalized product distribution $D(v',j'|1,10)$ and state-to-state reaction probabilities $P^R_{v'j'}$ vs final rotational quantum number j' for the $O + H_2$ reaction with $J = 0$ for initial state (1,10) at energy $E_{thr} = 1.66$ eV.

III B. Channel-selected specificities for $H+H_2$

To learn whether these trends, which we discussed above for $O + H_2$, are an isolated phenomenon for that case or whether they might be more general, we present a similar

TABLE III. Internal energies E_{int} and state-selected threshold energies E_{thr} in electron-volts for selected initial and final states of the $O + H_2$ reaction.

Initial states				Final states							
v	j	E_{int}	E_{thr}	v'	j'	E_{int}	E_{thr}	v'	j'	E_{int}	E_{thr}
0	11	1.157	1.484	0	17	1.031	1.358	1	12	1.129	1.272
0	12	1.302	1.596	0	18	1.108	1.396	1	13	1.184	1.350
0	13	1.454	1.718	0	19	1.189	1.510	1	14	1.243	1.410
				0	20	1.274	1.594	1	15	1.306	1.484
				0	21	1.362	1.716	1	16	1.373	1.568
				0	22	1.453	1.848	1	17	1.444	1.646
								1	18	1.516	1.730
								1	19	1.596	1.844

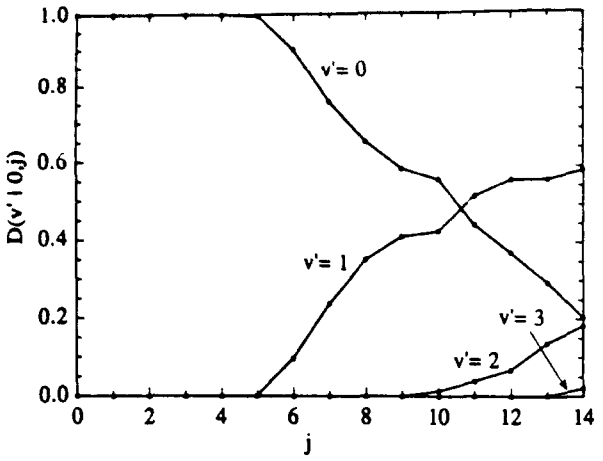

FIG. 3. Normalized product distributions $D(v'|0,j)$, which indicate the percentage of threshold reactive flux into each final vibrational level v' vs initial rotational quantum number j for initial states in the ground vibrational manifold at their threshold energies for the $O + H_2$ reaction with $J = 0$.

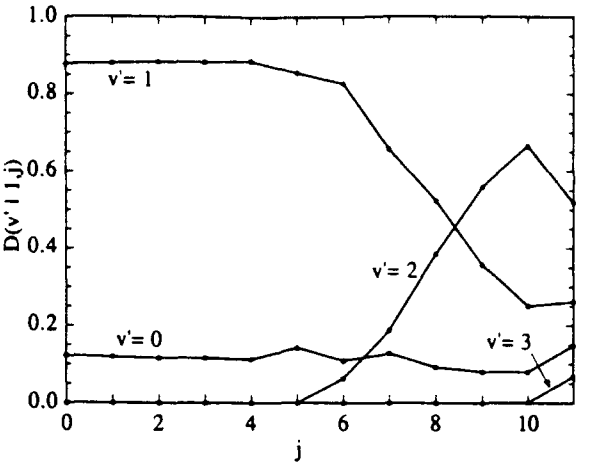

FIG. 4. Normalized product distributions $D(v'|1,j)$, which indicate the percentage of threshold reactive flux into each final vibrational level v' vs initial rotational quantum number j for initial states with $v = 1$ at their threshold energies for the $O + H_2$ reaction with $J = 0$.

study for the $H + H_2$ reaction. Results at the fully specified channel level are summarized in Tables IV–VI. For $J = 0$, where channels and states are the same, three initial states with different reaction thresholds were arbitrarily selected for study [(0,4), (1,4), and (0,10)]. It is seen in Table III that threshold flux for these states is very final-state specific; in each case, a single final state accounts for over 25% of the reactive flux, two states account for over 50%, and at most five are needed to account for 75% of the flux. The largest state-to-state reaction probabilities are all vibrationally adiabatic.

In order to test whether these trends also prevail for nonzero values of the total angular momentum, we evaluated results of the $H + H_2$ reaction at $J = 4$. Since for nonzero J both values of the parity are possible, results for $J = 4$, $P = +1$ and for $J = 4$, $P = -1$ are summarized separately in Tables V and VI, respectively.

There are many more channels for $J = 4$ than for $J = 0$, since l can vary from $\min(j-4,0)$ to $j+4$ for a given value of j. Nevertheless, the value of $N(x\%)$ remains small; the flux out of initial channels is quite final-channel specific. For example, Table VII shows channel-to-channel reaction probabilities for initial channels (0,10,6) and (0,10,8) and final channels (0,8,l') and (0,9,l') for all allowed values of the final-channel orbital angular momentum quantum number l' for $JP = 4+$. For a given initial channel and final state, one of the channel-to-channel reaction probabilities is larger than the others by more than an order of magnitude. For example, for initial channel (0,10,6), the channel-to-channel reaction probability into final channel (0,8,12), $P^R_{(0,10,6)(0,8,12)}$, is 0.106, but $P^R_{(0,10,6)(0,8,l')}$ is less than 0.01 for $l' = 4, 6, 8$, or 10. Similarly, the largest value of l' (13) dominates reaction out of initial channel (0,10,6) into final state (0,9). The data for other final states also show that reactants in initial channel (0,10,6) react preferentially to form products with the highest allowed value of l' for a given v' and j'. Table VII shows that for initial channel (0,10,8), the second highest value of l' for a given v' and j' is preferred. A similar trend is found for the other initial channels (0,10,l) with different values of l, so that a general summary of this propensity for (0,10,l) initial channels would be $j_i - l_i = -(j_f - l_f)$, where i and f denote initial and final.

III C. State-selected specificities for $H+H_2$

As mentioned above, state-selected and channel-selected specificities are the same for $J = 0$. Although our primary

TABLE IV. Final-state specificity of reaction out of selected initial states for the $H + H_2$ reaction with $J = 0$.

				25%		50%		75%					
(v,j)	E_{thr} (eV)	$E_{rel,thr}$ (eV)	N_{open}	N	F	N	F	N	F	Dominant (v',j'), $D(v',j'\|v,j)$[a]			
(0,4)	0.87	0.47	14	1	0.07	2	0.14	4	0.29	(0,4) 31	(0,3) 21	(0,5) 17	(0,0) 12
(1,4)	1.18	0.27	20	1	0.05	2	0.10	5	0.25	(1,3) 33	(1,4) 24	(1,1) 6	(0,0) 5
(0,10)	1.49	0.48	31	1	0.03	2	0.06	4	0.13	(0,10) 37	(0,9) 29	(0,8) 6	(1,7) 5

[a] The four final states which contribute most to $P^R_{v'}$ and their normalized conditional probabilities expressed as percentages, $D(v',j'|v,j) \times 100\%$, listed in order of the size of $D(v',j'|v,j)$, beginning with the greatest contributor.

TABLE V. Final-channel specificity of reaction out of selected initial channels for the H + H_2 reaction with $JP = 4+$.

(v,j,l)	E_{thr} (eV)	$E_{rel,thr}$ (eV)	N_{open}	25% N	25% F	50% N	50% F	75% N	75% F	75% Dominant (v',j',l'), $D(v',j',l'\|v,j,l)$[a]			
(0,4,0)	0.900	0.50	51	2	0.04	4	0.08	8	0.16	(0,2,6) 19	(0,1,5) 16	(0,3,7) 14	(0,0,4) 8
(0,4,2)	0.900	0.50	51	2	0.04	3	0.06	7	0.14	(0,2,6) 19	(0,1,5) 18	(0,3,7) 13	(0,0,4) 11
(0,4,4)	0.900	0.50	51	2	0.04	5	0.10	9	0.18	(0,3,5) 15	(0,4,6) 14	(0,4,4) 12	(0,5,5) 8
(0,4,6)	0.900	0.50	51	2	0.04	4	0.08	10	0.20	(0,4,4) 15	(0,3,5) 13	(0,4,6) 12	(0,5,5) 10
(0,4,8)	0.900	0.50	51	2	0.04	5	0.10	10	0.20	(0,5,1) 15	(0,4,0) 12	(0,3,1) 9	(0,6,2) 8
(1,4,0)	1.205	0.29	81	3	0.04	5	0.06	11	0.14	(1,2,6) 12	(1,1,5) 12	(1,3,1) 12	(1,4,0) 8
(1,4,2)	1.205	0.29	81	2	0.03	5	0.06	13	0.16	(1,1,5) 13	(1,2,6) 13	(1,0,4) 9	(1,3,7) 8
(1,4,4)	1.205	0.29	81	2	0.03	5	0.06	13	0.16	(1,3,5) 16	(1,4,4) 10	(1,3,3) 9	(1,4,6) 9
(1,4,6)	1.205	0.29	81	2	0.03	5	0.06	15	0.19	(1,3,5) 16	(1,4,4) 11	(1,3,3) 9	(1,2,4) 8
(1,4,8)	1.205	0.29	81	3	0.04	7	0.09	14	0.17	(1,2,6) 11	(0,8,4) 9	(1,3,7) 8	(1,1,5) 7
(0,10,6)	1.500	0.49	126	1	0.01	3	0.02	5	0.04	(0,8,12) 31	(0,9,13) 19	(0,7,11) 17	(1,6,10) 7
(0,10,8)	1.500	0.49	126	1	0.01	2	0.02	6	0.05	(0,9,11) 29	(0,8,10) 23	(0,10,12) 9	(1,6,8) 5
(0,10,10)	1.500	0.49	126	2	0.02	3	0.02	9	0.07	(0,9,9) 25	(0,10,10) 23	(0,8,8) 10	(0,9,11) 5
(0,10,12)	1.500	0.49	126	1	0.01	2	0.02	8	0.06	(0,10,8) 32	(0,9,7) 18	(0,11,9) 8	(0,10,10) 4
(0,10,14)	1.500	0.49	126	1	0.01	2	0.02	6	0.05	(0,10,6) 30	(0,11,7) 27	(0,9,5) 8	(1,8,4) 4

[a] The four final channels which contribute most to P_n^R and their normalized conditional probabilities expressed as percentages, $D(v',j',l'|v,j,l) \times 100\%$, listed in order of the size of $D(v',j',l'|v,j,l)$, beginning with the greatest contributor.

TABLE VI. Final-channel specificity of reaction out of selected initial channels for the H + H_2 reaction with $JP = 4-$.

(v,j,l)	E_{thr} (eV)	$E_{rel,thr}$ (eV)	N_{open}	25% N	25% F	50% N	50% F	75% N	75% F	75% Dominant (v',j',l'), $D(v',j',l'\|v,j,l)$[a]			
(0,4,1)	0.900	0.50	37	2	0.05	5	0.14	8	0.22	(0,3,6) 16	(0,2,5) 16	(0,4,7) 9	(0,3,6) 8
(0,4,3)	0.900	0.50	37	2	0.05	4	0.11	7	0.19	(0,2,5) 17	(0,3,6) 15	(0,2,3) 11	(0,1,4) 10
(0,4,5)	0.900	0.50	37	2	0.05	4	0.11	6	0.16	(0,2,5) 17	(0,2,3) 17	(0,1,4) 14	(0,3,4) 11
(0,4,7)	0.900	0.50	37	3	0.08	5	0.14	9	0.24	(0,2,5) 11	(0,4,3) 11	(0,3,2) 11	(0,2,3) 9
(1,4,1)	1.205	0.29	61	2	0.03	5	0.08	9	0.15	(1,3,2) 15	(1,2,3) 14	(1,2,5) 9	(1,3,6) 9
(1,4,3)	1.205	0.29	61	2	0.03	4	0.07	8	0.13	(1,2,3) 18	(1,3,2) 15	(1,1,4) 10	(1,2,5) 9
(1,4,5)	1.205	0.29	61	2	0.03	3	0.05	9	0.15	(1,2,3) 18	(1,1,4) 18	(1,2,5) 15	(1,3,2) 8
(1,4,7)	1.205	0.29	61	2	0.03	5	0.08	12	0.20	(1,2,5) 17	(1,1,4) 11	(1,3,6) 9	(0,8,5) 7
(0,10,7)	1.500	0.49	95	1	0.01	2	0.02	5	0.05	(0,8,11) 29	(0,9,12) 25	(0,7,10) 10	(1,6,9) 7
(0,10,9)	1.500	0.49	95	1	0.01	3	0.03	8	0.08	(0,9,10) 29	(0,8,9) 16	(0,10,11) 14	(1,7,8) 6
(0,10,11)	1.500	0.49	95	1	0.01	3	0.03	10	0.11	(0,10,9) 26	(0,9,8) 22	(0,9,10) 5	(0,10,11) 5
(0,10,13)	1.500	0.49	95	1	0.01	3	0.03	8	0.08	(0,10,7) 33	(0,11,8) 16	(0,9,6) 13	(1,8,5) 4

[a] The four final channels which contribute most to P_n^R and their normalized conditional probabilities expressed as percentages, $D(v',j',l'|v,j,l) \times 100\%$, listed in order of the size of $D(v',j',l'|v,j,l)$, beginning with the greatest contributor.

TABLE VII. Channel-to-channel reaction probabilities for initial channels (0,10,6) and (0,10,8) and final channels (0,8,l') and (0,9,l') for all allowed values of the final-channel orbital angular momentum quantum number l' for the H + H_2 reaction with $JP = 4+$.

v'	j'	l'	$P^R_{(0,10,6)n'}$[a]	$P^R_{(0,10,8)n'}$[a]
0	8	4	5.28(−4)[b]	7.62(−6)
0	8	6	4.29(−6)	4.44(−4)
0	8	8	1.30(−5)	2.28(−3)
0	8	10	1.32(−3)	5.41(−2)
0	8	12	1.06(−1)	2.44(−3)
0	9	5	8.96(−5)	1.07(−6)
0	9	7	3.06(−6)	9.35(−5)
0	9	9	8.03(−6)	1.55(−3)
0	9	11	8.22(−4)	6.79(−2)
0	9	13	6.31(−2)	2.16(−3)

[a] $P^R_{(n,j,l)n'}$ indicates channel-to-channel reaction probability $P^R_{nn'}$ for initial channel $n = (v,j,l)$.

[b] Numbers in parentheses are powers of ten.

emphasis here is on the completely resolved channel-selected level of detail, Table VIII presents the $J = 4$ results for H + H_2 in a state-selected way. Here up to nine l values contribute to the results for a given initial state, and up to nine final l' values are included for a given final state.

For $J = 4$, as for $J = 0$, threshold reactivity, even when averaged over l values, is highly final-state specific. At most two final states are required to account for 25% of the flux, and about five states account for over 75% of the flux. To a large extent, the same final states dominate state-selected threshold reactivity for both values of J. For initial states (0,4) and (1,4), three of the four final states that contribute most to $P^R_{\gamma\gamma'}$ are the same as for $J = 0$, although their ordering according to relative importance may differ. Two of the four dominant final states for initial state (0,10) are common to both $J = 0$ and 4.

The $J = 0$ reaction tends to be somewhat more final-state specific than the $J = 4$ reaction, as evidenced by the

TABLE VIII. Final-state specificity of reaction out of selected initial states for the H + H_2 reaction with $J = 4$.

(v,j)	E_{thr} (eV)	$E_{rel,thr}$ (eV)	N_{open}	25% N	25% F	50% N	50% F	75% N	75% F	Dominant (v',j'), $D(v',j'\|v,j)$*			
(0,4)	0.900	0.50	14	2	0.14	3	0.21	4	0.29	(0,3) 25	(0,2) 21	(0,4) 21	(0,1) 13
(1,4)	1.205	0.29	20	2	0.10	3	0.15	6	0.30	(1,3) 23	(1,2) 19	(1,4) 15	(1,1) 11
(0,10)	1.500	0.49	31	1	0.03	3	0.10	5	0.16	(0,9) 25	(0,8) 23	(0,10) 14	(0,7) 8

*The four final states which contribute most to P_γ^A and their normalized conditional probabilities expressed as percentages, $D(v',j'|v,j) \times 100\%$, listed in order of the size of $D(v',j'|v,j)$, beginning with the greatest contributor.

slightly lower values of $N(x\%)$ and slightly higher values of $D(v',j'|v,j)$ for $J = 0$ than for $J = 4$. The vibrational level specificity of the $J = 0$ and 4 reactions is the same for initial states (0,4) and (1,4) [100% of the flux is into $v' = 0$ for (0,4); 22% is into $v' = 0$ and 78% is into $v' = 1$ for (1,4)]. Vibrationally nonadiabatic processes account for a slightly larger fraction of the reactive flux for initial state (0,10) when $J = 4$ than when $J = 0$ (86%, 10%, and 4% of the flux is into $v' = 0$, 1, and 2, respectively, for $J = 0$; 82%, 18%, and 0% is into $v' = 0$, 1, and 2 for $J = 4$).

III D. Above threshold specificity

Although the main emphasis of the present study is on specificity at threshold, we also investigated briefly, for comparison, how the final-state specificity of state-selected reactivity changes as energy is increased above threshold. Table IX summarizes such a study for initial state (0,5) of the O + H_2 reaction with $J = 0$ in the energy range 0.70–1.90 eV. As the energy is increased above threshold (0.89 eV), the state-selected reactivity becomes less final-state specific. By 1.90 eV, the four most important final states account for less than 25% of the total reactive flux, and the 22 most important final states account for less than 75% of the flux, whereas at the threshold energy, two final states contribute more than 25% of the flux, and four final states contribute more than 75% of the flux. This behavior of initial state (0,5) at high energy also stands in contrast to threshold reactivity summarized in Tables I and II. For example, at the highest-energy threshold studied, that for initial state (0,14) at 1.86 eV, over 25% of the state-selected flux goes into a single final state (1,19).

In Figs. 5(a) and 5(b), $N(x\%)$ and $F(x\%)$ are plotted vs the total energy at threshold. Figure 5(a) indicates that final-state specificity is greatest at the state-selected reaction threshold. Both above *and below* threshold, the reaction is less specific. [Even at energies below the threshold for initial state (0,5), there is still a small probability of reaction.] Above about 0.90 eV, final-state specificity as indicated by $N(x\%)$ and $D(v',j'|0,5)$ (Table IX) decreases markedly; the number of small contributors increases dramatically with energy, as indicated by the large value of $N(75\%)$ at high energies. Although the specificity does decrease at energies above threshold, some specificity remains. For example, five final channels still account for 25% of the flux at 1.90 eV, and Fig. 5(b) emphasizes that the *fraction* of final states [$F(x\%)$] that account for a given percentage of the flux does not necessarily increase with energy above threshold. At 1.90 eV, the fraction is 0.06 for 25% of the flux, as compared to 0.08 at threshold.

Up to 1.90 eV, the four largest state-to-state reaction probabilities for reaction out of (0,5) are all vibrationally

TABLE IX. Final-state specificity of reaction out of initial state ($v = 0, j = 5$) for the O + H_2 reaction with $J = 0$.

E_{tot} (eV)	E_{rel} (eV)	N_{open}	25% N	25% F	50% N	50% F	75% N	75% F	Dominant (v',j'), $D(v',j'\|0,5)$*			
0.70	0.21	12	2	0.17	4	0.33	6	0.50	(0,6) 17	(0,5) 16	(0,7) 15	(0,4) 13
0.80	0.31	16	2	0.13	3	0.19	5	0.31	(0,8) 22	(0,9) 22	(0,7) 16	(0,10) 14
0.90	0.41	23	2	0.09	3	0.13	4	0.17	(0,10) 23	(0,9) 23	(0,11) 16	(0,8) 15
1.00	0.51	27	2	0.07	3	0.11	6	0.22	(0,10) 20	(0,11) 19	(0,9) 14	(0,12) 12
1.10	0.61	30	2	0.07	4	0.13	9	0.30	(0,11) 18	(0,10) 16	(0,12) 12	(0,9) 10
1.20	0.71	34	2	0.06	5	0.15	11	0.32	(0,11) 16	(0,12) 13	(0,10) 12	(0,9) 5
1.30	0.81	43	3	0.07	8	0.19	15	0.35	(0,11) 11	(0,12) 9	(0,10) 7	(0,5) 5
1.40	0.91	49	4	0.08	10	0.20	17	0.35	(0,11) 7	(0,15) 7	(0,12) 6	(0,14) 6
1.50	1.01	53	4	0.08	10	0.19	17	0.32	(0,15) 8	(0,14) 8	(0,2) 6	(0,3) 5
1.60	1.11	58	3	0.05	8	0.14	18	0.31	(0,15) 9	(0,14) 8	(0,2) 8	(0,1) 7
1.70	1.21	68	3	0.04	8	0.12	18	0.26	(0,15) 9	(0,2) 9	(0,14) 8	(0,1) 8
1.80	1.31	76	4	0.05	10	0.13	21	0.28	(0,2) 8	(0,1) 8	(0,15) 6	(0,14) 6
1.90	1.41	79	5	0.06	11	0.14	23	0.29	(0,2) 8	(0,1) 8	(0,17) 6	(0,15) 6

*The four final states which contribute most to P_γ^A and their normalized conditional probabilities expressed as percentages, $D(v',j'|0,5) \times 100\%$, listed in order of the size of $D(v',j'|0,5)$, beginning with the greatest contributor.

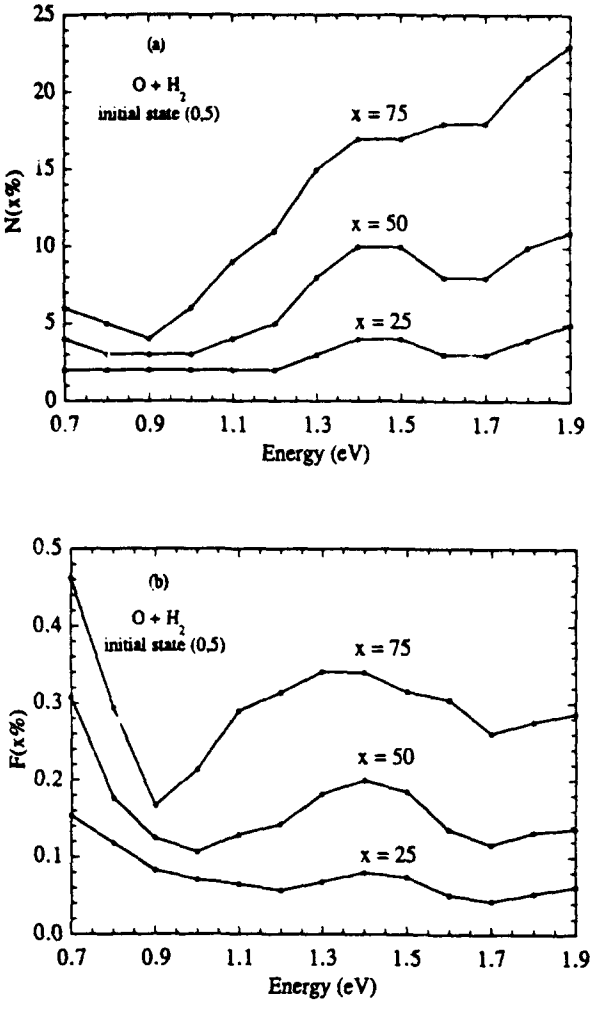

FIG. 5. For the $O + H_2$ reaction with $J = 0$ (a) the minimum number $N(x\%)$ of state-to-state reaction probabilities needed to account for $x\%$ of the flux out of initial state (0,5) vs energy for $x = 25$, 50, and 75; (b) the fraction $F(x\%) = N(x\%)/N_{open}$ vs energy for $x = 25$, 50, and 75.

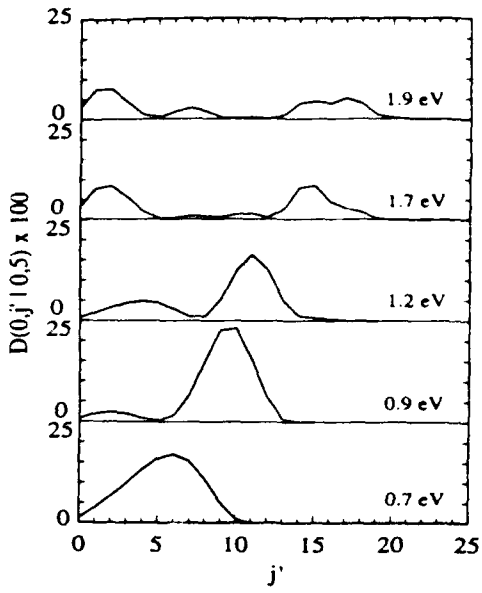

FIG. 6. Normalized product distributions $D(v', j'|0,5)$ vs final rotational quantum number j' for initial state (0,5) and final vibrational quantum number v' equal to 0 for five energies for the $O + H_2$ reaction with $J = 0$. The energies range from 0.2 eV below the state-selected threshold to 1.0 eV above it.

adiabatic, in contrast to the high degree of vibrational nonadiabaticity for the (0,14) and other high-j states at similar energies. At 1.86 eV, 57% of the reactive transitions out of (0,5) are vibrationally adiabatic, compared to only 21% out of (0,14).

Figure 6 shows how the product distribution specificities $D(v', j'|v, j)$ change with energy for initial state (0,5) and $v' = 0$, which is the dominant final vibrational level. At 0.7 eV, which is below the state-selected threshold of 0.89 eV, $D(0, j'|0,5)$ as a function of j' is a single, relatively broad peak with a maximum at $j' = 6$. By 0.9 eV, very close to the threshold energy, this peak has shifted to the right (the maximum is now at $j' = 10$) and grown both taller and narrower. At the same time, a second peak has begun to appear at low j'. This bimodal distribution is maintained as the energy is increased further. The peak at low j' becomes more pronounced with increasing energy, while the peak at high j' shifts to the right and grows broader. By 1.9 eV, the highest peak is the one at low j'. These trends are reflected in the dominant final states and their conditional probabilities given in Table IX. The broadening of the high-j' peak above threshold is reflected in the decreasing conditional probabilities, and the increasing bimodality of the distribution is evidenced by the fact that by 1.8 eV, (0,2) and (0,1) are the most important final states. Since the highest and most concentrated peak occurs at 0.9 eV, Fig. 6 supports the observation made above that state-selected reactivity is most specific at a state-selected threshold.

Another way to study trends in final-state specificity as energy is increased beyond threshold is to choose one energy and evaluate the final-state specificity of several states whose thresholds occur over a range of energies up to the chosen energy. This strategy has the advantage that the number of open final states remains constant. The results of such a study are depicted in Fig. 7 for initial states in the ground vibrational manifold at 1.86 eV. For initial states not too far above threshold ($j = 9$–14), $N(x\%)$ decreases regularly as the threshold is approached until $j = 14$, for which 1.86 eV is the threshold energy. For $j = 15$, whose threshold is above 1.86 eV, the reaction is *less specific* than for $j = 14$. Thus we find that for a given energy E, the final-state specificity is greatest for those initial states whose thresholds are at or very close to E, just as before we found that for a given initial state, the specificity is greatest at its threshold energy. This again confirms our conclusion that final-state specificity is especially large at state-selected reaction thresholds.

In Fig. 8, the fraction of reactive flux into each final vibrational level at 1.86 eV, given by the product distribution $D(v'|0, j)$, is plotted as a function of j for initial states in the ground vibrational manifold. For most of the range of j values, in particular for $j = 3$–12, we find that 50%–60% of the

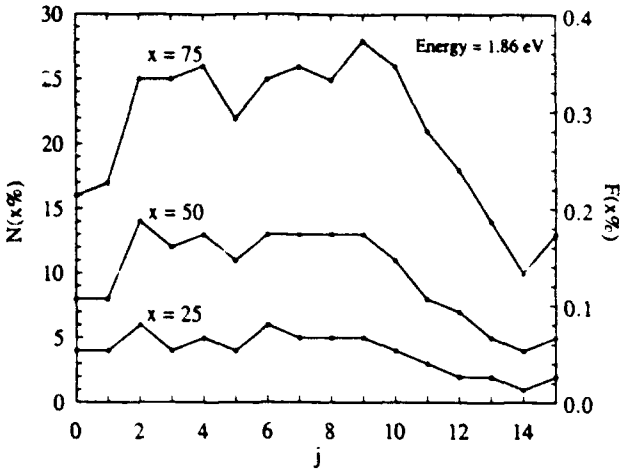

FIG. 7. The minimum number $N(x\%)$ of state-to-state reaction probabilities needed to account for $x\%$ of the reactive flux and fraction $F(x\%) = N(x\%)/N_{open}$ vs initial rotational quantum number j for initial states in the ground vibrational manifold for $x = 25$, 50, and 75 for the $O + H_2$ reaction with total energy 1.86 eV.

reactive flux is vibrationally adiabatic. At low values of j ($j = 0$–2), the degree of adiabaticity is more erratic, and for high j ($j = 13$ and 14), whose thresholds are near 1.86 eV, the degree of nonadiabaticity increases substantially.

IV. CONCLUDING REMARKS

A high degree of final-state specificity has been demonstrated for state-selected reactivity at energies near the state-selected reaction thresholds for the reactions $O + H_2 \rightarrow OH + H$ and $H + H_2 \rightarrow H_2 + H$. This specificity has been found for nonzero values of the total angular momentum J as well as for $J = 0$, and it is particularly marked for large values of the rotational quantum number.

We do not know of any previous study that has demonstrated the remarkable specificities that emerge from these accurate quantum dynamics calculations. The present results are particularly dramatic for $O + H_2$ because the final diatomic, OH, is not the same as the initial one, H_2, and yet the specificity is very strong. One might have been less surprised if such specificities were observed only in symmetric reactions such as $H + H_2$. The closest previously observed analog of this specificity seems to be associated with inelastic processes of the form $A + BC(v,j) \rightarrow A + BC(v',j')$, where indeed the initial and final diatomic *are* the same. For example, trajectory studies of several atom–diatom systems have shown a strong tendency for rotational energy changes to compensate vibrational energy changes.[9–19] High rotational levels were found to enhance vibrationally inelastic cross sections,[9–16] and the results show that the degree of final-state specificity increases with initial j for both vibrationally elastic and inelastic processes.[11–13,15] The most dramatic experimental examples are found in the work of Pritchard and co-workers[19,20] for rare gas collisions with Li_2. There the effect was seen for high initial j and low relative translational energies and it manifested itself, as in the trajectory studies, as a narrow distribution of final j' values for each final v'. Although those collisions are quite different from the reactive ones studied here, they might provide useful analogies to pursue in future work.

Another possible avenue of future study is to relate the final-state distributions to the properties of the transition state. If the transition state is viewed as a short-lived intermediate,[5,8,21] this viewpoint is similar to the transition-state–product-state overlap model of direct bimolecular reactions,[22] or to the interpretation of product rotational state distributions in photodissociation processes in terms of the properties of initial dissociative resonance states.[23] We have already applied this kind of analysis to some aspects of the product rotational distributions for the $H + H_2$ reaction,[8] and we believe that this kind of analysis should also be useful for understanding the high state-to-state specificity of near-threshold processes observed in the present study.

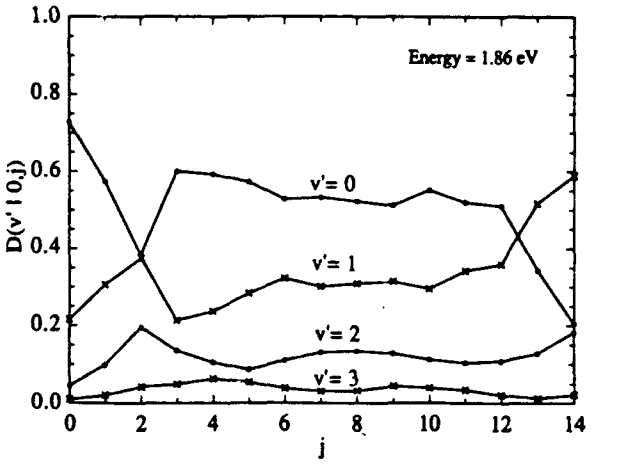

FIG. 8. Normalized product distributions $D(v'|0,j)$, which indicate the percentage of threshold reactive flux into each final vibrational level v' vs initial rotational quantum number j for initial states in the ground vibrational manifold at a total energy of 1.86 eV for the $O + H_2$ reaction with $J = 0$.

ACKNOWLEDGMENTS

The authors are grateful to Ronald S. Friedman for helpful contributions to this work. This work was supported in part by the National Science Foundation.

[1] W. A. Lester, Jr. and R. B. Bernstein, J. Chem. Phys. 53, 11 (1970).
[2] G. C. Schatz, J. Chem. Phys. 84, 2620 (1986); B. R. Johnson and N. W. Winter, *ibid.* 66, 4116 (1977).
[3] A. J. C. Varandas, F. B. Brown, C. A. Mead, D. G. Truhlar, and N. C. Blais, J. Chem. Phys. 86, 6258 (1987).
[4] D. W. Schwenke, K. Haug, D. G. Truhlar, Y. Sun, J. Z. H. Zhang, and D. J. Kouri, J. Phys. Chem. 91, 6080 (1987); D. W. Schwenke, K. Haug, M. Zhao, D. G. Truhlar, Y. Sun, J. Z. H. Zhang, and D. J. Kouri, *ibid.* 92, 3202 (1988); D. W. Schwenke, M. Mladenovic, M. Zhao, D. G. Truhlar, Y. Sun, and D. J. Kouri, in *Supercomputer Applications for Reactivity, Dynamics, and Kinetics of Small Molecules*, edited by A. Lagana (Kluwer, Dordrecht, 1989), p. 131; Y. Sun, C.-h. Yu, D. J. Kouri, D. W. Schwenke, P. Halvick, M. Mladenovic, and D. G. Truhlar, J. Chem. Phys. 91, 1643 (1989); D. G. Truhlar, D. W. Schwenke, and D. J. Kouri, J. Phys. Chem. 94, 7346 (1990).
[5] D. C. Chatfield, R. S. Friedman, D. G. Truhlar, B. C. Garrett, and D. W. Schwenke, J. Am. Chem. Soc. 113, 486 (1991).

[6] D. C. Chatfield, D. G. Truhlar, and D. W. Schwenke, J. Chem. Phys. **94**, 2040 (1991).
[7] D. C. Chatfield, R. S. Friedman, G. C. Lynch, D. G. Truhlar, and D. W. Schwenke (to be published).
[8] D. C. Chatfield, R. S. Friedman, D. G. Truhlar, and D. W. Schwenke, Faraday Discuss. Chem. Soc. **91**, 289 (1991).
[9] J. E. Dove, S. Raynor, and H. Teitelbaum, Chem. Phys. **50**, 175 (1980).
[10] N. C. Blais and D. G. Truhlar, in *Potential Energy Surfaces and Dynamics Calculations*, edited by D. G. Truhlar (Plenum, New York, 1981), p. 431.
[11] D. L. Thompson, J. Chem. Phys. **75**, 1829 (1981).
[12] D. L. Thompson, J. Phys. Chem. **86**, 630 (1982).
[13] N. C. Blais and D. G. Truhlar, J. Phys. Chem. **86**, 638 (1982).
[14] D. L. Thompson, J. Phys. Chem. **86**, 2538 (1982).
[15] D. L. Thompson, J. Chem. Phys. **76**, 5947 (1982).
[16] D. L. Thompson, Chem. Phys. Lett. **92**, 383 (1982).
[17] D. L. Thompson, J. Chem. Phys. **78**, 1763 (1983).
[18] P. D. Magill, B. Stewart, N. Smith, and D. E. Pritchard, Phys. Rev. Lett. **60**, 1943 (1988).
[19] B. Stewart, P. D. Magill, T. P. Scott, J. Derouard, and D. E. Pritchard, Phys. Rev. Lett. **60**, 282 (1988).
[20] K. L. Saenger, N. Smith, S. L. Dexheimer, C. Engelke, and D. E. Pritchard, J. Chem. Phys. **79**, 4076 (1983).
[21] O. Atabek, R. Lefebvre, M. Garcia Sucre, J. Gomez-Llorente, and H. Taylor, Int. J. Quantum Chem. **40**, 211 (1991); R. S. Friedman and D. G. Truhlar, Chem. Phys. Lett. **183**, 539 (1991); D. C. Chatfield, R. S. Friedman, D. W. Schwenke, and D. G. Truhlar, J. Phys. Chem. (to be published).
[22] For a review of such models, see R. E. Wyatt, in *Atom–Molecule Collision Theory*, edited by R. B. Bernstein (Plenum, New York, 1979), pp. 492–500.
[23] See, e.g., C. X. W. Qian, A. Ogai, L. Iwata, and H. Reisler, J. Chem. Phys. **92**, 4296 (1990); R. Schinke, A. Untch, H. U. Suter, and J. R. Huber, *ibid.* **94**, 7929 (1991).